Activation of endosomal dynein motors by stepwise assembly of Rab7–RILP–p150^{Glued}, ORP1L, and the receptor βIII spectrin

Marie Johansson,[1] Nuno Rocha,[2] Wilbert Zwart,[2] Ingrid Jordens,[2] Lennert Janssen,[2] Coenraad Kuijl,[2] Vesa M. Olkkonen,[1] and Jacques Neefjes[2]

[1]Department of Molecular Medicine, National Public Health Institute, Biomedicum, FI-00251 Helsinki, Finland
[2]Division of Tumor Biology, The Netherlands Cancer Institute, 1066CX Amsterdam, Netherlands

The small GTPase Rab7 controls late endocytic transport by the minus end–directed motor protein complex dynein–dynactin, but how it does this is unclear. Rab7-interacting lysosomal protein (RILP) and oxysterol-binding protein–related protein 1L (ORP1L) are two effectors of Rab7. We show that GTP-bound Rab7 simultaneously binds RILP and ORP1L to form a RILP–Rab7–ORP1L complex. RILP interacts directly with the C-terminal 25-kD region of the dynactin projecting arm p150^{Glued}, which is required for dynein motor recruitment to late endocytic compartments (LEs). Still, p150^{Glued} recruitment by Rab7–RILP does not suffice to induce dynein-driven minus-end transport of LEs. ORP1L, as well as βIII spectrin, which is the general receptor for dynactin on vesicles, are essential for dynein motor activity. Our results illustrate that the assembly of microtubule motors on endosomes involves a cascade of linked events. First, Rab7 recruits two effectors, RILP and ORP1L, to form a tripartite complex. Next, RILP directly binds to the p150^{Glued} dynactin subunit to recruit the dynein motor. Finally, the specific dynein motor receptor Rab7–RILP is transferred by ORP1L to βIII spectrin. Dynein will initiate translocation of late endosomes to microtubule minus ends only after interacting with βIII spectrin, which requires the activities of Rab7–RILP and ORP1L.

Introduction

The location and movement of intracellular vesiculotubular structures is controlled by microtubule-dependent kinesin and dynein motor proteins, as well as actin-dependent myosin motor proteins. Microtubule-based vesicle motility usually occurs in a bidirectional, stop-and-go manner because of the alternating activities of kinesin motors for plus-end movement and dynein motors for minus-end movement toward the microtubule organizing center (MTOC; Hirokawa, 1998; Wubbolts et al., 1999; Vale, 2003). How motor proteins are targeted to individual vesicles, how they dock on specific receptors, and how motor activity is controlled in a spatial and temporal manner are all processes that are poorly understood.

Cytoplasmic dynein is an ∼1.2-MD multisubunit protein complex, and it is the major motor for centripetal transport of membranous cargoes along microtubules (Schroer et al., 1989). Dynactin, which is also an ∼1.2-MD multisubunit complex, is a critical component of most, if not all, of the cytoplasmic dynein–driven activities. Dynactin participates in motor binding to microtubules (Waterman-Storer et al., 1995), increases motor processivity (King and Schroer, 2000; Culver-Hanlon et al., 2006), and acts as a multifunctional adaptor connecting cargo and dynein motor (Karki and Holzbaur, 1999; Schroer, 2004). At least 15 subunits of the dynein–dynactin motor are identified. The 1-MD dynein heavy chain dimer and the 300-kD p150^{Glued} dimer of the projecting arm of dynactin contact microtubules (Culver-Hanlon et al., 2006). p150^{Glued} is connected to the dynein heavy chain via the dynein intermediate chains (Waterman-Storer et al., 1995) and increases dynein motor processivity (King and Schroer, 2000; Culver-Hanlon et al., 2006). The actin-related protein 1 (Arp1) subunit forms a short filament at the base of dynactin and can bind membrane-associated βIII spectrin, which probably acts as the membrane receptor for the dynein–dynactin motor complex (Holleran et al., 2001; Muresan et al., 2001). αIβIII spectrin is located on the cytosolic side of late endocytic compartments (LEs), Golgi, and other subcellular compartments (De Matteis and Morrow, 2000),

M. Johansson and N. Rocha contributed equally to this paper.

Correspondence to Jacques Neefjes: j.neefjes@nki.nl

Abbreviations used in this paper: Arp, actin-related protein; FLIM, fluorescence lifetime imaging microscopy; FRET, fluorescence resonance energy transfer; LE, late endocytic compartment; MIIC, major histocompatibility complex class II–containing compartment; MBP, maltose-binding protein; mRFP, monomeric red fluorescent protein; MTOC, microtubule organizing center; ORD, oxysterol-binding protein–related domain; ORP, oxysterol-binding protein–related protein; RILP, Rab7-interacting lysosomal protein; shRNA, short hairpin RNA.

The Journal of Cell Biology, Vol. 176, No. 4, February 12, 2007 459–471
http://www.jcb.org/cgi/doi/10.1083/jcb.200606077

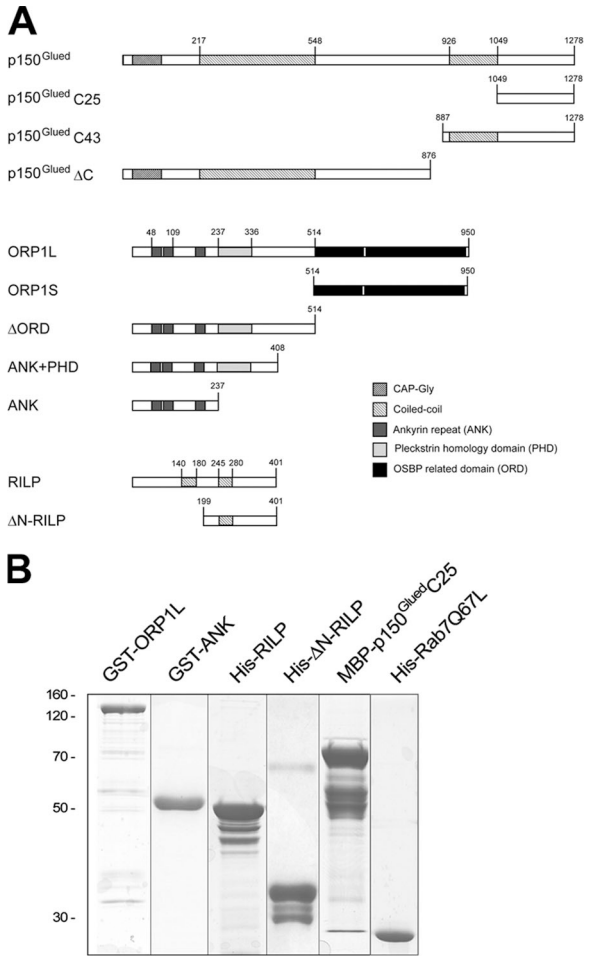

Figure 1. **The ORP1L, RILP, and p150^{Glued} constructs and purified recombinant proteins.** (A) Schematic representation of the constructs used in this study. The domains in ORP1L and p150^{Glued} are indicated. RILP contains predicted coiled-coil regions only. Numbers indicate amino acid residue positions. (B) Purified fusion proteins were resolved by 10% SDS-PAGE and Coomassie stained. Positions of the molecular weight markers and the fusion proteins are indicated.

implying that compartment-selective dynein motor recruitment cannot be controlled by βIII spectrin itself.

Small GTPases of the Rab family are present on specific subcellular compartments to regulate vesicle transport and fusion. They are ideal candidates for orchestrating the spatiotemporal regulation of motor-driven vesicle trafficking. Several Rab GTPases have been shown to interact directly or indirectly with motor proteins. These include members of the kinesin motor family (Rab4, Rab5, and Rab6), the dynein motor (Rab6 and Rab7), and the myosin motors (Rab8, Rab11, and Rab27a; Jordens et al., 2005). Rab6, which regulates Golgi transport, requires the effector bicaudal-D1 and -D2 (BicD1/2) to interact with the p50^{dynamitin} subunit of dynactin (Hoogenraad et al., 2003; Matanis et al., 2002) or a third protein, egalitarian (Egl), which directly interacts with the dynein light chain in *Drosophila melanogaster* (Navarro et al., 2004). An activation state–dependent interaction of Rab6 with p150^{Glued} has also been observed in a directed two-hybrid analysis (Short et al., 2002). We have studied another Rab protein, Rab7, which, through its effector Rab7-interacting lysosomal protein (RILP), recruits the dynein–dynactin motor to LEs, resulting in minus end–driven vesicular transport to the MTOC (Jordens et al., 2001). The Rab7–RILP–dynein motor cascade has been shown to act on many Rab7-containing compartments, including *Salmonella*-containing phagosomes (Harrison et al., 2004; Marsman et al., 2004), early melanosomes (Jordens et al., 2006), major histocompatibility complex class II–containing compartments (MIICs; Jordens et al., 2001), and cytolytic granules (Stinchcombe et al., 2006). The crystal structure of Rab7 in complex with a C-terminal domain of RILP revealed the details of this interaction. RILP forms a coiled-coil homodimer with two symmetric surfaces that bind two separate Rab7–GTP molecules to form a tetrameric complex (Wu et al., 2005), which has been confirmed in biochemical experiments (Colucci et al., 2005; Marsman et al., 2006). The recent finding that a member of the oxysterol-binding protein–related protein (ORP) family, ORP1L, also interacts with Rab7 and induces clustering of LEs (Johansson et al., 2005) complicated a simple interpretation of Rab7–RILP–controlled dynein motor recruitment. ORPs have been implicated in diverse aspects of cellular processes, including sterol and phospholipid metabolism, vesicle transport, and cell signaling (Lehto and Olkkonen, 2003). The mechanisms by which ORP proteins contribute to these processes have, however, remained largely unknown. We recently showed that ORP1L localizes to LEs and interacts via its ankyrin repeat region with the small GTPase Rab7 (Johansson et al., 2005). ORP1L was shown to stabilize the GTP-bound active form of Rab7 on LEs and to affect the subcellular distribution of these organelles, analogously, to RILP (Jordens et al., 2001). A third Rab7 effector, Rabring7 (Mizuno et al., 2003), clusters LEs, much like the other effectors, and induces lysosomal acidification, but dynein motor recruitment has not been shown. Surprisingly, no obvious sequence similarity is found between the three Rab7 effectors.

Apparently, multiple effectors interact with Rab7. They could be mutually exclusive, but they may also interact simultaneously with this Rab GTPase. How the Rab7 effector complexes recruit the dynein motor complex is also unclear. We have studied the interaction of RILP and ORP1L with the Rab7 GTPase, as well as their interactions with dynein–dynactin motor subunits. We show that Rab7 is part of a tripartite complex binding RILP and ORP1L simultaneously. RILP is essential for dynein motor recruitment through a direct interaction with the C-terminal portion of the p150^{Glued} subunit of the dynein–dynactin motor. ORP1L recruits this complex to βIII spectrin domains, which appears to be critical for dynein motor activation and minus-end transport of LEs. Rab7, thus, recruits two proteins with diverse functions in the control of dynein motor–driven transport: RILP for motor binding and ORP1L for transport to the membrane-associated late endocytic βIII spectrin receptor for motor activation. The dynein–dynactin motor, thus, requires two receptors before actively transporting LEs to the microtubule minus end. Its projecting arm, p150^{Glued}, is recruited by RILP bound by active Rab7 in LE membranes. The other Rab7 effector, ORP1L, then transfers the Rab7–RILP–p150^{Glued}–dynein motor complex to βIII spectrin interacting with the base of the dynactin complex Arp1. Only after completion of this "mass protein action" does the dynein motor transport LEs to the microtubule minus end.

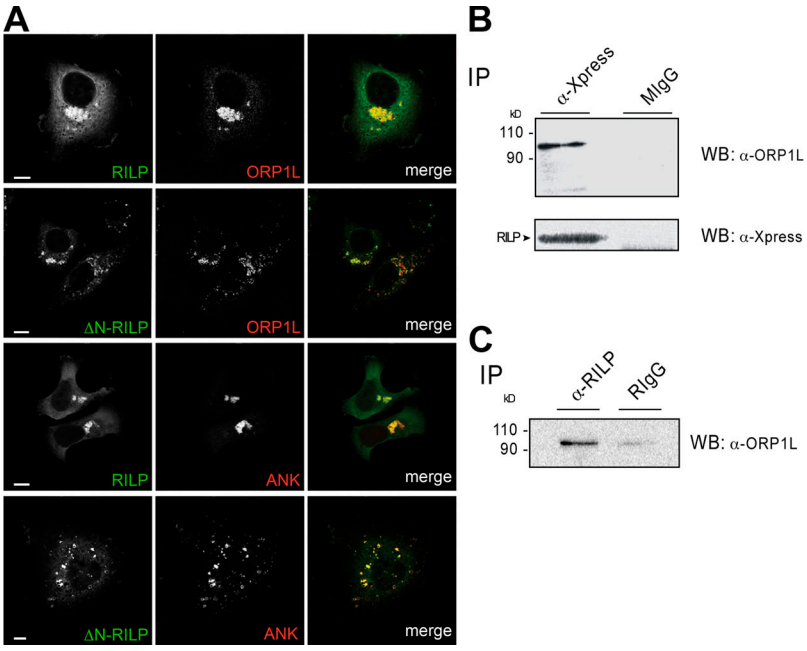

Figure 2. **ORP1L and RILP colocalize and are part of a physical complex.** (A) ORP1L and RILP colocalize on juxtanuclear late endocytic clusters. HeLa cells were transfected with GFP–RILP or GFP–ΔN-RILP, together with Xpress-tagged ORP1L or Xpress-tagged ORP1L–ANK domain (red), as indicated in the images. ANK and ORP1L colocalize with RILP or ΔN-RILP (right, merge). Bars, 10 μm. (B) ORP1L co-isolates with expressed RILP. HeLa cells were transfected with Xpress-tagged RILP and immunoprecipitated with anti-Xpress antibody (α-Xpress) or irrelevant mouse IgG (MIgG). The isolates were Western blotted with anti-ORP1L antibodies (WB: α-ORP1L). (bottom) Corresponding lanes probed with anti-Xpress antibody (WB: α-Xpress). (C) Coimmunoprecipitation of endogenous RILP and ORP1L. HeLa cell lysates were immunoprecipitated with rabbit anti-RILP serum (α-RILP) or irrelevant rabbit IgG (RIgG). The isolates were Western blotted with anti-ORP1L antibodies (WB: α-ORP1L).

Results

ORP1L and RILP colocalize on juxtanuclear late endocytic clusters as part of a physical complex

Both RILP and ORP1L have been reported to localize on LEs, and their overexpression induces juxtanuclear clustering of these compartments, suggesting involvement in microtubule-dependent LE motility (Jordens et al., 2001; Johansson et al., 2005). We studied the distribution of GFP-tagged RILP and Xpress-tagged ORP1L expressed in HeLa cells, and we visualized the proteins by confocal laser-scanning fluorescence microscopy. The proteins showed extensive colocalization on compact juxtanuclear organelle clusters (Fig. 2 A). We studied the contribution of their various domains to this phenotype (Fig. 1 A). The N-terminal portion of ORP1L, consisting of the ankyrin repeat region (ANK; aa 1–237; Fig. 2 A) or the ANK and the PH domain regions (ANK + PH; aa 1–408; not depicted), displayed colocalization with RILP similar to that of full-length ORP1L (Fig. 2 A), demonstrating that the N-terminal Rab7-interacting ANK region of ORP1L suffices to specify this localization. We have previously shown that the ANK and ANK + PH domain regions of ORP1L induce clustering of LEs in the absence of ectopically expressed RILP (Johansson et al., 2003, 2005). We tested whether a truncated RILP that fails to recruit the dynein–dynactin motor, but still binds to the switch and interswitch regions of small GTPase Rab7 (ΔN-RILP; Jordens et al., 2001; Wu et al., 2005), affects the LE-clustering phenotype induced by the ORP1L ANK domain (Fig. 2 A). Overexpression of ΔN-RILP inhibited clustering by ANK, although the two proteins still colocalized on the scattered LEs.

To determine whether ORP1L and RILP might interact physically, HeLa cells were transected with Xpress-tagged RILP and subjected to immunoprecipitation with the Xpress mAb or irrelevant mouse IgG. Western blotting of the isolates with anti-ORP1L antibody revealed coprecipitation of endogenous ORP1L with Xpress-RILP (Fig. 2 B). To study the interaction in an endogenous setting, HeLa cell lysates were incubated with anti-RILP antibody or irrelevant rabbit IgG. Endogenous ORP1L was detected in the immunoprecipitates by Western blotting (Fig. 2 C), suggesting that ORP1L and RILP not only colocalize on LEs but are also part of a physical complex in cells.

ORP1L and RILP interactions with Rab7 in living cells

We then applied fluorescence resonance energy transfer (FRET) techniques to test whether a RILP–Rab7–ORP1L interaction could be visualized in living cells using fluorescently labeled proteins. When two fluorophores are in close proximity (<8 nm) and the fluorophores show spectral overlap, FRET can occur (Förster, 1948). FRET can be detected by sensitized emission (when the acceptor emits light at the cost of donor fluorescence) or fluorescence lifetime imaging microscopy (FLIM). FLIM detects the time between photon absorbance by the donor fluorophore and its emission (in nanoseconds), which decreases when energy is transferred to acceptor fluorophores. FLIM, which, in principle, is more quantitative than sensitized emission for detecting FRET and FRET efficiencies (Wallrabe and Periasamy, 2005), was applied to study interactions between Rab7, RILP, and ORP1L in living HeLa cells.

HeLa cells transfected with GFP–RILP and monomeric red fluorescent protein (mRFP)–Rab7, GFP–ORP1L and mRFP–Rab7, or GFP–ORP1L and mRFP–RILP, were analyzed by FLIM, and the lifetime of the GFP fluorophore was measured. The cells were cocultured with Mel JuSo cells stably expressing histone 2B (H2B)–GFP, which were used as an internal null FRET control. Because RILP and Rab7 have been previously shown to interact (Cantalupo et al., 2001; Jordens et al., 2001) and cocrystallize (Wu et al., 2005), these proteins constituted a positive control for the experimental setup.

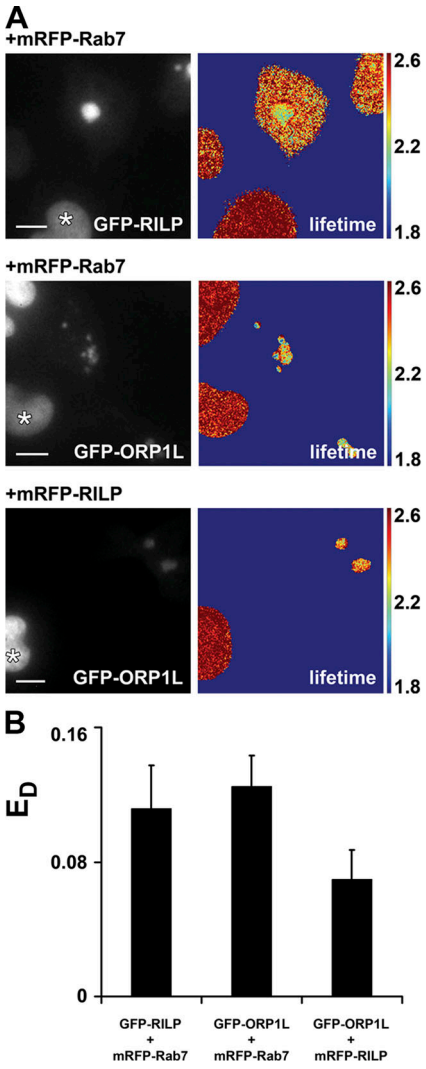

Figure 3. **FRET between ORP1L, Rab7, and RILP.** (A) HeLa cells were transfected with GFP–RILP or GFP–ORP1L and cotransfected with mRFP–Rab7 or mRFP–RILP, as indicated. The transfected HeLa cells were cocultured with Mel JuSo cells stably expressing H2B–GFP (indicated by *) as an internal marker with a lifetime of 2.6 ns. (left) Wide-field image of the transfected and internal control cells. (right) FLIM image of the same cells, in which the fluorescence lifetime is depicted in false colors. The color scale with the respective lifetimes (in nanoseconds) is indicated. The fluorescence lifetime of GFP–RILP or GFP–ORP1L was determined on vesicles immobile during data acquisition (~12 s). Bar, 10 μm. (B) The donor FRET efficiencies (E_D) between the GFP- and mRFP-tagged proteins were determined and plotted in the bar diagram. Mean ± the SD. $n > 20$.

When GFP–RILP and mRFP–Rab7 were coexpressed, discrete perinuclear clusters were formed. A substantial decrease in GFP fluorescence lifetime on the GFP–RILP–positive structures was observed in the presence of mRFP–Rab7. The measured lifetime was 2.29 ± 0.06 ns (Fig. 3 A), when the lifetime for H2B–GFP in control cells (indicated by an asterisk) was at 2.56 ± 0.03 ns (Bastiaens and Squire, 1999). The calculated donor FRET efficiency, or E_D (see Materials and methods), between GFP–RILP and mRFP–Rab7 was 11.2 ± 2.5% (Fig. 3 B), indicating efficient FRET and close spacing of RILP and Rab7 in living cells. Measuring FLIM between GFP–ORP1L and mRFP–Rab7 resulted in a comparable reduced lifetime of the GFP fluorophore, 2.23 ± 0.03 ns (Fig. 3 A), corresponding to an E_D of 12.5 ± 1.85% (Fig. 3 B).

To determine whether ORP1L and RILP are in close proximity not only to Rab7 but also to each other, FLIM was performed between GFP–ORP1L and mRFP–RILP. The decrease of fluorescence lifetime was somewhat less pronounced, but still significant (2.35 ± 0.04 ns; E_D = 7.0 ± 1.8%; Fig. 3, A and B). Similar results were obtained when measuring FRET by sensitized emission (unpublished data). These data suggest that ORP1L is part of the same complex as RILP and Rab7. The absolute distances between the proteins cannot, however, be determined from these data because FRET efficiency is not only determined by the Förster distance (distance between the fluorescent groups) but also by the orientation factor and flexibility of the fluorophores (Förster, 1948).

The Rab7–RILP–ORP1L tripartite complex

Having established that ORP1L and RILP are part of a physical complex (Fig. 2, A and B), we set out to study the interaction between the two proteins by a series of pull-down experiments. Endogenous RILP was pulled down from HeLa cell lysate using purified, matrix-immobilized GST–ORP1L (Fig. 4 A). To study whether this interaction between ORP1L and RILP is direct, we used purified His_6-tagged RILP or the constitutively active GTP-loaded Rab7 mutant Q67L, which is produced in *E. coli*, to pull down purified GST–ORP1L. These experiments revealed that, although His_6–Rab7Q67L efficiently pulled down GST–ORP1L in accordance with our previous results (Johansson et al., 2005), no interaction was detected between His_6–RILP and GST–ORP1L (Fig. 4 B). Because both RILP and ORP1L bind to Rab7, we next tested, using purified proteins, whether Rab7 is able to bridge the two effectors and thereby form a tripartite complex. Because soluble full-length recombinant GST–ORP1L is produced in limiting amounts, GST–ANK, which suffices to bind Rab7 and can be efficiently produced, was used to perform the binding assay. GST fusion proteins of the Rab7-interacting ORP1L ANK fragment (GST–ANK) were incubated with His_6–RILP, GTP-loaded His_6–Rab7Q67L, or a mixture of both His_6-tagged proteins. As expected, GST–ANK pulled down His_6–Rab7Q67L, but not His_6–RILP. However, His_6–RILP was pulled down by GST–ANK when the incubation was performed in the presence of GTP-loaded His_6–Rab7Q67L (Fig. 4 C). This indicated that Rab7 is required to bridge RILP and ORP1L, and that the two effectors do not compete for the same binding site on Rab7.

To test whether ORP1L and RILP interacted cooperatively with Rab7, we immobilized GTP-loaded GST–Rab7 and pulled down in vitro–translated and radiolabeled ORP1L or RILP. This experiment was performed in the presence of a step gradient of increasing amounts of purified RILP, ΔN-RILP, or ORP1L fusion proteins, respectively. GTP-loaded GST–Rab7 pulled down ^{35}S-labeled ORP1L to a significant extent in the absence of RILP, but further addition of His_6–RILP to the reaction mixture increased ORP1L binding to Rab7 in a dose-dependent manner. ^{35}S-labeled ORP1L binding to immobilized Rab7 increased up to approximately fourfold in the presence of His_6–RILP (Fig. 4, D [I] and E). Addition of His_6–RILP had no effect

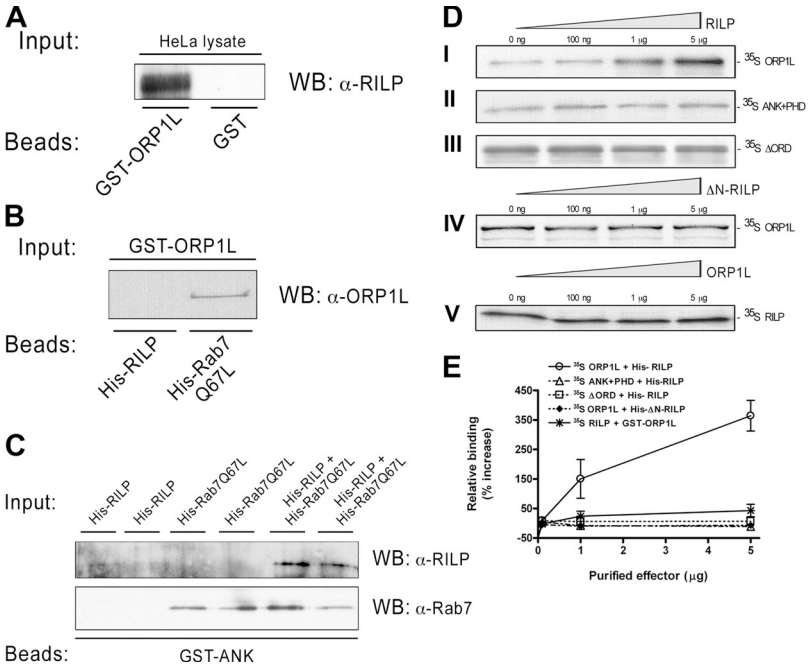

Figure 4. **The ORP1L–Rab7–RILP heterotrimeric complex.** (A) Proteins were pulled down from HeLa cell lysates with GST–ORP1L or GST and Western blotted with anti-RILP antiserum (WB: α-RILP). Pull-down assays were performed with purified proteins. (B) His_6–RILP or His_6–Rab7Q67L were immobilized on a matrix and used to pull down GST–ORP1L. Isolates were Western blotted with anti-ORP1L antibodies (WB: α-ORP1L). (C) GST–ORP1L ANK fragment (GST–ANK) was immobilized and incubated with His_6–RILP, GTP-loaded His_6–Rab7Q67L, or a mixture containing both His_6–RILP and GTP-loaded His_6–Rab7Q67L. The material pulled down by the ANK fragment was Western blotted with antibodies against Rab7 or RILP (indicated on the right). Duplicate samples are shown for each condition. (D) RILP enhances ORP1L binding to Rab7. GST–Rab7 was immobilized on a matrix, loaded with GTP, and incubated with in vitro–translated ^{35}S-labeled ORP1L in the presence of increasing amounts of His_6–RILP. ^{35}S-labeled ORP1L protein pulled down by GST–Rab7 was visualized by SDS-PAGE and autoradiography (I). Similar pull-down experiments were performed with in vitro–translated ^{35}S-labeled ORP1L ANK + PHD (II) or ^{35}S-labeled ORP1L ΔORD fragments (III). Pull-down of full-length ^{35}S-labeled ORP1L by active GST–Rab7 in the presence of increasing amounts of His_6–ΔN-RILP (indicated above the lanes) (IV). A reciprocal pull-down experiment in which in vitro–translated ^{35}S-labeled RILP was incubated with immobilized His_6–Rab7–GTP in the presence of increasing amounts of GST–ORP1L (indicated above the lanes; V). (E) Quantification of the radioactive bands in D by phosphorimaging. The plotted data shows the relative increase in binding of in vitro–translated proteins to immobilized Rab7–GTP in the presence of a step-gradient of effector proteins. Binding of ORP1L to Rab7 was enhanced up to fourfold in the presence of RILP. The plotted data represents the mean of three independent experiments ± the SD (error bars).

on the binding of ORP1L ANK (not depicted) or ANK + PHD fragments to Rab7–GTP (Fig. 4, D [II] and E). To further map the region of ORP1L involved in the observed stabilization, we extended the ANK + PHD domain to contain a region upstream of the oxysterol-binding protein–related domain (ORD) displaying a high probability of forming a coiled coil (ΔORD; Fig. 1 A; Lupas et al., 1991; Berger et al., 1995). Also this construct failed to produce the effect observed with full-length ORP1L (Fig. 4, D [III] and E), suggesting that the ORD of ORP1L is involved in the stabilization effect observed in the presence of His_6–RILP.

To determine if the N-terminal region of RILP, which is required for dynein–dynactin motor recruitment to LEs (Jordens et al., 2001), is necessary for facilitating the ORP1L–Rab7 interaction, the pull-down experiment with GTP-loaded Rab7 was repeated with in vitro–translated ^{35}S-labeled ORP1L in the presence of His_6–ΔN-RILP. This truncated form of RILP failed to increase ORP1L binding to Rab7–GTP (Fig. 4, D [IV] and E), demonstrating that the same domain of RILP essential in dynein–dynactin motor recruitment to LEs (Jordens et al., 2001) is also involved in the stabilization of the Rab7–ORP1L interaction.

To test if the observed cooperativity of ORP1L binding to Rab7 in the presence of RILP is reciprocal, we pulled down in vitro–translated ^{35}S-labeled RILP with immobilized His_6–Rab7–GTP, followed by incubation with increasing amounts of GST–ORP1L. RILP was observed to bind to immobilized Rab7, but the addition of GST–ORP1L had no effect on RILP binding (Fig. 4, D [V] and E). These experiments suggest that RILP might stabilize the Rab7–ORP1L interaction in a unidirectional manner, and again indicate that binding of the two effectors to Rab7 is not mutually exclusive.

RILP-Rab7 recruits p150^{Glued} to LEs, whereas ORP1L is required for actual minus-end transport

GTP-loaded Rab7 collects RILP and ORP1L into a complex, and then recruits the dynein–dynactin motor protein complex to LE membranes. The dynein–dynactin motor complex interacts via the Arp1 filament with the β chain of membrane-associated αIβIII spectrin (Holleran et al., 2001), which thereby acts as a membrane receptor for the motor. Fluorescence microscopy analyses performed in HeLa cells demonstrated that the dynein–dynactin motor subunits Arp1, p50^{dynamitin} (not depicted), and p150^{Glued} were selectively recruited to LEs by myc-tagged RILP (Fig. 5 A). ΔN-RILP, in contrast, failed to recruit these dynein–dynactin motor subunits (Fig. 5 B).

To identify the dynein–dynactin motor subunit required for the RILP-mediated targeting to LEs, we tested whether ectopically expressed RILP or ORP1L could selectively stabilize particular dynein–dynactin motor subunits on LE membranes when the dynein–dynactin motor complex is dissociated. Overexpression of (GFP–)p50^{dynamitin} displaces the projecting arm of dynactin from the rest of the dynactin complex, leaving Arp1 membrane associated, whereas p150^{Glued} and other more distal dynein–dynactin motor subunits are dispersed in the cytosol (Echeverri et al., 1996; Burkhardt et al., 1997; Eckley et al., 1999). GFP–p50^{dynamitin} was overexpressed in HeLa cells in the absence or presence of HA-RILP or Xpress–ORP1L. Cells were fixed and stained for endogenous p150^{Glued} (Fig. 5 C). Expression of RILP alone, but not ORP1L (or ANK; unpublished data), sufficed to rescue p150^{Glued} localization on LEs when the dynein motor complex was dissociated by p50^{dynamitin} overexpression. It is noteworthy that the dynein–dynactin motor

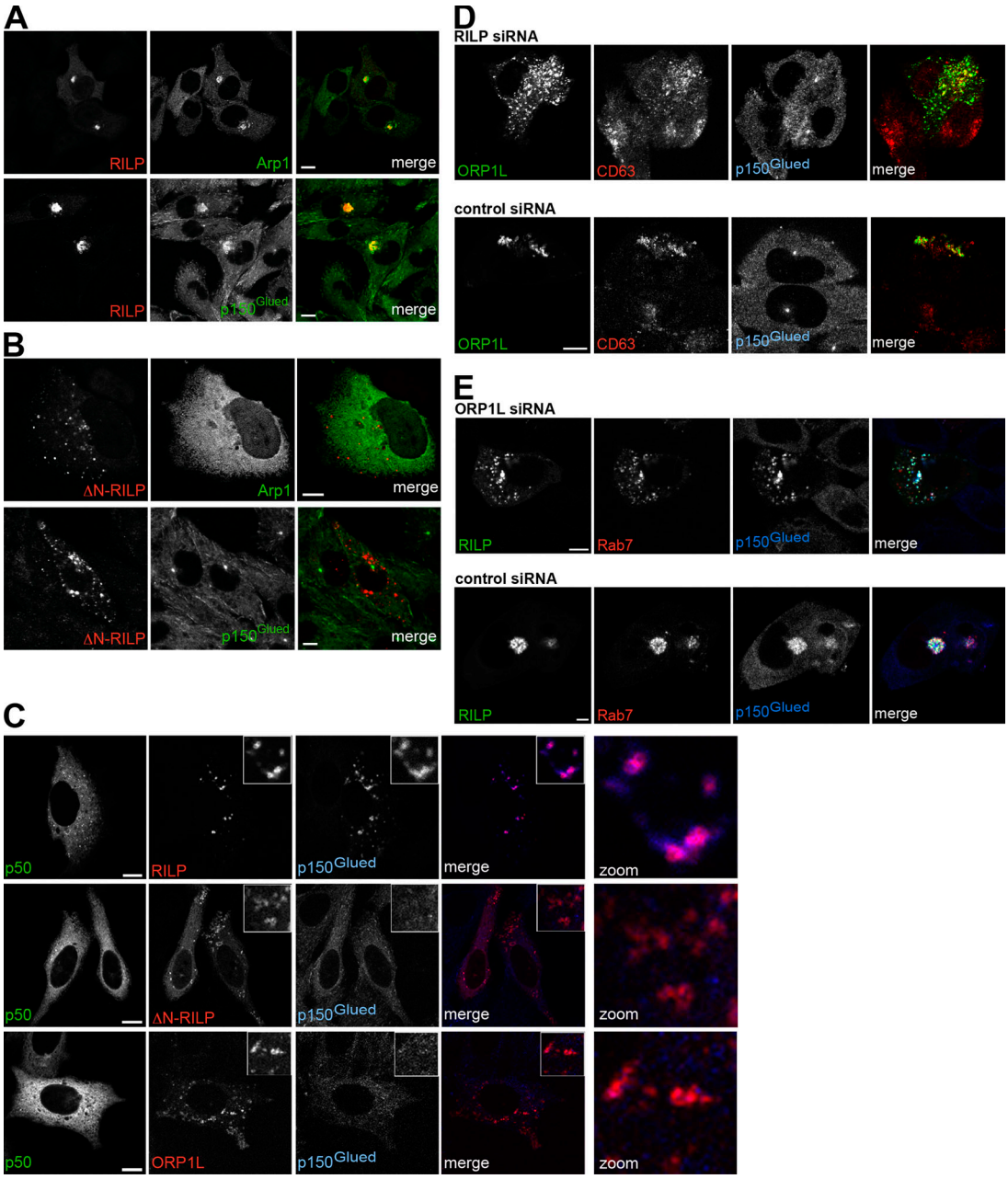

Figure 5. **Role of RILP and ORP1L in the recruitment of the p150^{Glued} subunit of the dynein–dynactin motor.** (A) HeLa cells were transfected with myc-tagged RILP (red), and the location of GFP–Arp1 and endogenous p150^{Glued} (green) was determined. (B) HeLa cells were transfected with VSV-tagged ΔN-RILP (red), and the location of GFP–Arp1 or endogenous p150^{Glued} (green) was determined. (C) HeLa cells were transfected with p50^{dynamitin} (green) and HA-tagged RILP, ΔN-RILP, or ORP1L (red), and subsequently stained for endogenous p150^{Glued} (blue), as indicated. The merge and the magnified merge (zoom) images only show the stainings in the red and blue images. (D) HeLa cells were transfected with GFP–ORP1L (green) and RILP siRNA or scrambled siRNA, as indicated. At 72 h after transfection, cells were fixed and stained for endogenous CD63 (red) and p150^{Glued} (blue). The merge shows only the ORP1L and CD63 labeling. (E) HeLa cells were transfected with GFP–RILP (green), mRFP–Rab7 (red), and ORP1L siRNA or a scrambled siRNA, as indicated, and fixed at 48 h after transfection. Cells were stained for endogenous p150^{Glued} (blue). Bars, 10 μm.

complex is no longer assembled into a functional motor when p50^{dynamitin} is overexpressed, resulting in scattered vesicles still containing RILP and p150^{Glued}. To further test the involvement of endogenous RILP or ORP1L in motor recruitment and minus end–directed transport, the proteins were down-regulated by specific siRNAs, and the localizations of RILP (ectopically expressed), ORP1L (ectopically expressed), late endocytic markers, and p150^{Glued} were determined (Fig. 5, D and E). Down-regulation of endogenous RILP or ORP1L induced scattering of LEs. p150^{Glued} was recruited to the scattered vesicles only when RILP was overexpressed (Fig. 5 E). Importantly, p150^{Glued} recruitment by RILP in the absence of ORP1L did not suffice to drive minus-end transport of LEs into a characteristic perinuclear cluster around the MTOC (Fig. 5 E). This suggests that RILP, but not ORP1L, interacts with the p150^{Glued} subunit of the dynein–dynactin motor complex. However, interactions

of RILP or ORP1L with other stabilizing motor subunits, or the involvement of additional proteins linking p150^{Glued} and RILP, cannot be excluded by these experiments.

RILP interacts with the C-terminal domain of p150^{Glued}

To identify the potential interaction between RILP and p150^{Glued}, we first determined the p150^{Glued} region recruited by RILP. ΔC, the GFP-tagged N-terminal 95-kD fragment of p150^{Glued} (aa 1–876) was coexpressed with mRFP–RILP (Fig. 6 A). Although decorating microtubules and the MTOC, this fragment failed to be recruited to the RILP cluster. This suggested that RILP interacts (directly or indirectly) with the C-terminal 55-kD portion of p150^{Glued}. The coiled coil–containing region in p150^{Glued} CC2 (aa 887–1,063) also failed to be recruited by RILP (not depicted), whereas GFP–p150^{Glued} C25 (aa 1,049–1,278), representing the most C-terminal 25-kD region after the coiled coil, was recruited to the mRFP–RILP cluster (Fig. 6 A). This construct did not colocalize with mRFP–ΔN-RILP (Fig. 6 A), in agreement with the observation that this dominant-negative RILP variant inhibits p150^{Glued} recruitment to LEs (Fig. 5, B–D; Jordens et al., 2001). These data suggest that the N-terminal half of RILP interacts with the most C-terminal region of p150^{Glued} to recruit the dynein–dynactin motor complex to LEs. To test whether this p150^{Glued} fragment also inhibited minus-end transport by acting as a dominant-negative dynein motor fragment, analogously to overexpression of p50^{dynamitin} (Burkhardt et al., 1997), the GFP-tagged versions of both proteins were overexpressed in HeLa cells, and late endocytic structures were visualized by labeling with anti-CD63 antibodies (Fig. 6 B). Overexpression of the C-terminal fragment of p150^{Glued} induced a mild, but reproducible, scattering of LEs, whereas the effect of p50^{dynamitin} overexpression was considerably more pronounced. This suggests that overexpression of the (presumably) monomeric version of the p150^{Glued} C-terminal fragment competes weakly with the endogenous p150^{Glued} homodimer for binding to the RILP homodimer.

A direct interaction between RILP and the most C-terminal region of p150^{Glued} can only be studied using purified proteins. GST–Rab7, GST–ORP1L, maltose-binding protein (MBP)–p150^{Glued} C25, His$_6$–RILP, and His$_6$–ΔN-RILP were expressed in *E. coli* and purified. GST–Rab7 was immobilized on beads and loaded with GTPγS. To reconstitute the tripartite complex in vitro, the beads were subsequently loaded with His$_6$–RILP or His$_6$–ΔN-RILP in the presence or absence of ORP1L. The beads were washed, and equal amounts of purified MBP–p150^{Glued} C25 were added to all reactions before another washing step. To determine specific binding, which is binding-dependent on the active GTP-bound conformation of Rab7, GTPγS was eluted by EDTA and replaced by excess GDP. The eluates were then incubated with amylose resin to capture the MBP–p150^{Glued} C25 fusions before extensive washing. The bound fractions were analyzed by SDS-PAGE and Western blotting (Fig. 6 C). Only RILP, but not ΔN-RILP or ORP1L, was recovered from the amylose-bound MBP–p150^{Glued} C25 fractions, in line with the observations above. This interaction was also reproduced in the absence of immobilized Rab7, suggesting that the

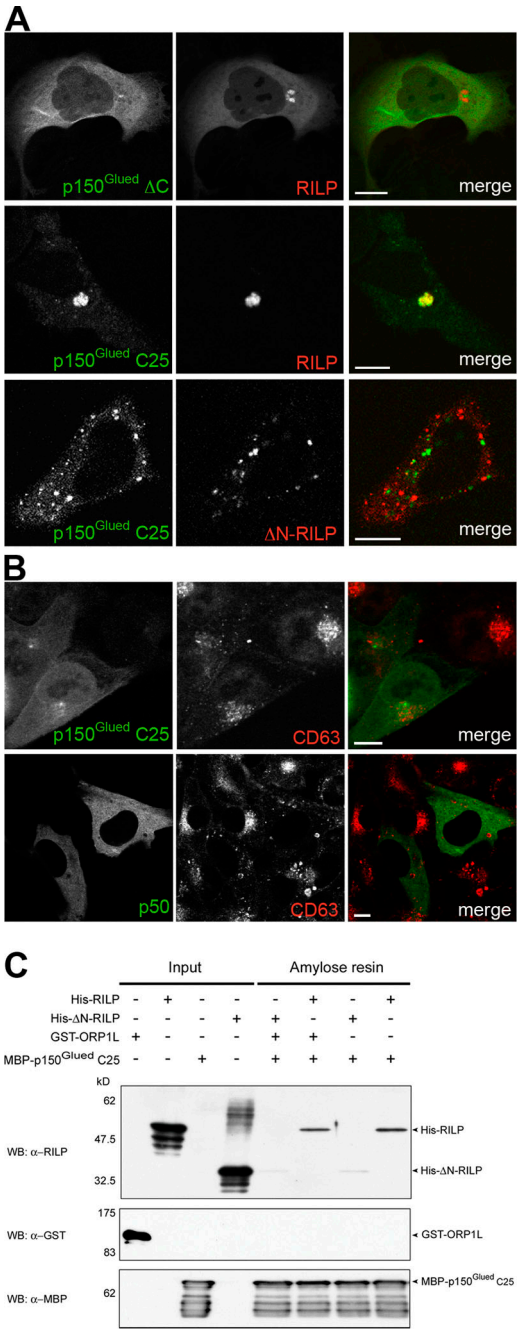

Figure 6. **RILP interacts with the C-terminal 25-kD fragment of p150^{Glued}.** (A) HeLa cells were transfected with mRFP–RILP or mRFP-tagged ΔN-RILP, along with GFP-tagged ΔC and C25 fragments of p150^{Glued}. (B) HeLa cells were transfected with GFP–p150^{Glued} C25 or GFP–p50^{dynamitin}, fixed, and stained with anti-CD63 antibodies. (C) Purified GTPγS-loaded Rab7Q67L coupled to GST-beads was incubated with combinations of purified RILP, ΔN-RILP, ORP1L, or p150^{Glued} C25 (aa 1,049–1,278), as indicated above the gels. Proteins bound in a GTP-dependent manner were eluted with EDTA and the C-terminal MBP–p150^{Glued} fragments (C25) were captured on amylose resin. The input and resin-bound proteins were Western blotted with anti-RILP, -GST, or -MBP antibodies. Bars, 10 μm.

GTPase is not required for binding in vitro of p150^{Glued} to RILP (unpublished data). These results support a model in which the C-terminal domain of RILP interacts with active GTP-loaded Rab7 and the N-terminal domain of RILP (which is absent in

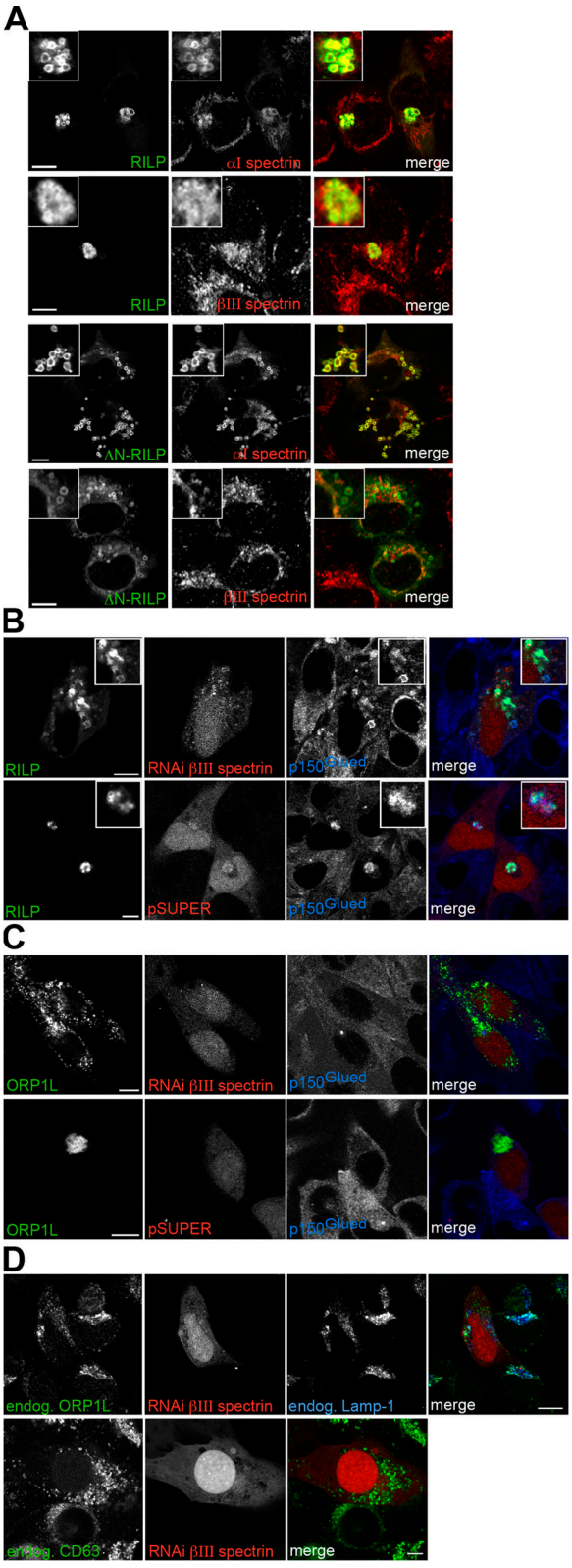

Figure 7. **αIβIII spectrin localizes to LEs for ORP1L-mediated RILP–p150^{Glued}–driven minus-end transport.** (A) Mel JuSo cells were transfected with GFP–RILP or GFP–ΔN-RILP for 48 h before fixation and staining for αI spectrin or βIII spectrin. αI and βIII spectrin (red) are located on RILP- and ΔN-RILP–labeled vesicles, as well as other subcellular structures. Note that βIII spectrin labeling localizes differently within the GFP–RILP– or GFP–ΔN-RILP–labeled vesicles. (insets) Magnification of vesicles showing the localization of RILP or ΔN-RILP and αI spectrin or βIII spectrin. (B) HeLa cells were transfected with GFP–RILP and pSUPER vector coexpressing mRFP and a control or βIII spectrin shRNA. Cells were fixed at 72 h after transfection and stained for endogenous p150^{Glued} (blue). (C) HeLa cells were transfected with GFP–ORP1L and pSUPER vector coexpressing mRFP and a control or βIII spectrin shRNA. At 72 h after transfection, cells were fixed and stained for endogenous p150^{Glued} (blue). (D) Endogenous ORP1L and spectrin. HeLa cells were transfected with a βIII spectrin shRNA pSUPER construct coexpressing mRFP. At 72 h after transfection, cells were fixed and stained for endogenous ORP1L (green) or endogenous CD63 (green) and the late endocytic marker Lamp-1 (blue). Bars, 10 μm.

ΔN-RILP) interacts with the C-terminal 25-kD fragment of the dynein–dynactin motor subunit p150^{Glued}.

ORP1L recruits the Rab7–RILP–p150^{Glued} complex to the membrane-associated receptor βIII spectrin

If the Rab7–RILP complex recruits the dynein motor through the p150^{Glued} stalk, it could act as a second dynein motor receptor in parallel with βIII spectrin on the membrane of LEs. βIII spectrin has an N-terminal actin-binding domain that interacts with the base of the dynein–dynactin motor Arp1 (Holleran et al., 2001) and is required for anchoring this motor to the membrane and for motor activity (Muresan et al., 2001). αIβIII spectrin is likely to be the only spectrin family member present on LEs (Stankewich et al., 1998; De Matteis and Morrow, 2000). To test whether αIβIII spectrin is located on LEs, and whether RILP or the dominant-negative form ΔN-RILP affects spectrin localization, we introduced GFP-tagged RILP or ΔN-RILP in Mel JuSo cells and stained these with antibodies for αI or βIII spectrin (Fig. 7 A). αI and βIII spectrin localized to various subcellular structures, including RILP- and ΔN-RILP–containing vesicles. Although full-length RILP was required for p150^{Glued} recruitment, αIβIII spectrin remained membrane associated, even when ΔN-RILP was expressed. The membrane association of αIβIII spectrin is, thus, independent of RILP, and probably occurs through association with various (unidentified) late endocytic transmembrane proteins and phospholipids (De Matteis and Morrow, 2000).

If RILP and βIII spectrin are receptors for the same motor protein, do they act in concert or independently? HeLa cells were transfected with GFP–RILP and a pSUPER construct that coexpresses mRFP and a control or βIII spectrin short hairpin RNA (shRNA). The cells were fixed and stained for endogenous p150^{Glued}. Although (GFP–)RILP recruited p150^{Glued}, down-regulation of βIII spectrin prevented transport of the RILP–p150^{Glued}–positive vesicles to the microtubule minus ends, which is similar to the situation observed after down-regulation of ORP1L (Fig. 7 B and Fig. 5 E). We subsequently tested whether the clustering of LEs imposed by ORP1L was also dependent on βIII spectrin. HeLa cells were transfected with GFP–ORP1L– and pSUPER vector–coexpressing mRFP and control or βIII spectrin shRNA. Cells were fixed and stained for p150^{Glued} (Fig. 7 C). GFP–ORP1L clustered vesicles without recruiting detectable p150^{Glued}, which is in accordance with the finding that RILP is responsible for recruiting p150^{Glued}. Silencing of βIII spectrin expression resulted in scattering of ORP1L-positive vesicles, implying that minus-end transport of ORP1L

and RILP-positive vesicles requires βIII spectrin (Fig. 7, B and C). Unlike RILP, endogenous ORP1L was detectable with the available antibodies. We tested whether down-regulation of βIII spectrin also induced scattering of organelles positive for endogenous ORP1L and other late endocytic markers. HeLa cells were transfected with the pSUPER vector coexpressing mRFP and a shRNA for βIII spectrin before labeling (Fig. 7 D). Scattering of the ORP1L-, Lamp-1–, and CD63-positive LEs was only detected in the mRFP-expressing transfected cells. These results suggest that βIII spectrin is required for minus-end transport of LEs labeled with endogenous or ectopically expressed ORP1L (Fig. 7, C and D). Notably, silencing of βIII spectrin (Fig. 7 B), as well as ORP1L (Fig. 5 E), prevents LEs labeled with Rab7–RILP–$p150^{Glued}$ complexes to be actively transported to the minus end of microtubules.

Discussion

Most intracellular organelles are transported along microtubules in a bidirectional manner, driven by at least two oppositely directed motor proteins. Late endosomes, like MIICs, move bidirectionally by the alternating activities of the dynein–dynactin motor (for minus-end transport) and the kinesin motor (for plus-end transport; Wubbolts et al., 1999). The function of motor proteins must be spatially and temporally coordinated to explain this complex pattern of organelle motility. We show how minus-end transport of LEs by the dynein–dynactin motor is regulated by the tripartite complex ORP1L–Rab7–RILP. We show that RILP directly interacts with the 25-kD C-terminal region of $p150^{Glued}$. This explains how activation of Rab7, via RILP, recruits the dynein–dynactin motor to LEs. However, we also show that this motor recruitment does not suffice for minus-end microtubular transport of LEs. ORP1L is presumably essential for translocation of Rab7–RILP–$p150^{Glued}$ to βIII spectrin, which acts as the general dynein receptor on LEs and other organelles (De Matteis and Morrow, 2000). Only then does dynein motor–driven minus-end transport ensue. Rab7–RILP is the late endocytic–specific dynein motor receptor that cooperates with the general dynein receptor βIII spectrin for active dynein motor activity on LEs. This $p150^{Glued}$–RILP–Rab7–ORP1L–βIII spectrin cascade explains one critical step in the spatiotemporal control of late endocytic motility.

βIII spectrin pairs with αI spectrin and the αIβIII spectrin heterodimer localizes to the cytosolic side of LEs, Golgi, and other organelles (Stankewich et al., 1998; De Matteis and Morrow, 2000). However, its presence does not suffice to recruit the dynein motor. Instead, activation of Rab7 specifies the target membrane for RILP- and ORP1L-mediated dynein–dynactin motor activities rather than the more ubiquitous spectrin receptor. Several Rab proteins have recently been found to control motor proteins either via a direct interaction or via effector proteins (Jordens et al., 2005). In all cases, it is unclear whether additional membrane motor receptors on specific compartments are also involved in RabGTPase-controlled, motor-driven transport.

We define a novel interaction where Rab7 recruits RILP to interact with the C terminus of $p150^{Glued}$. This may stabilize the projecting motor arm on the dynein–dynactin base comprised of Arp1, $p50^{dynamitin}$, and other subunits (Schroer, 2004). The C-terminal fragment of $p150^{Glued}$ also interacts with dynein intermediate chain and Arp1 (Kumar et al., 2001) in a manner that still leaves space for RILP interactions. That RILP interacts with a fragment near the dynein–dynactin motor base is not unexpected because the Rab7–RILP complex is membrane embedded and not likely to protrude far from the membrane. We have previously failed to detect this by cryoelectronmicroscopy (Jordens et al., 2001), probably because of the inefficiency of immunolabeling.

In this study, we have used a series of techniques to study the interaction between Rab7 and two of its effectors, RILP and ORP1L. The FRET results indicate that Rab7, RILP, and ORP1L are in close proximity in living cells, and our in vitro experiments indicate that RILP and ORP1L can bind simultaneously to the same active GTP-loaded Rab7 molecule. In fact, the binding of ORP1L to Rab7 is stabilized by RILP. The N-terminal ANK region of ORP1L specifies the Rab7 interaction (Johansson et al., 2005). We now show that the ANK region binds directly to active GTP-loaded Rab7, but additional determinants in the C-terminal half of ORP1L stabilize the RILP–Rab7–ORP1L tripartite complex. Because the crystal structure of the Rab7–RILP complex revealed that two GTP-loaded Rab7 molecules bind on opposite sides of a RILP homodimer (Wu et al., 2005), the RILP–Rab7–ORP1L complex is probably a heterotrimeric dimer with ORP1L positioned at the boundaries of the complex (Fig. 8).

How does the RILP–Rab7–ORP1L complex recruit the dynein motor to LEs? Rab7 associates with LEs after GTP binding and recruits the effectors RILP and/or ORP1L, thus forming a tripartite complex. In theory, both effectors could mediate the recruitment of the motor. When we overexpressed $p50^{dynamitin}$ to dissociate the dynein–dynactin motor complex such that the $p150^{Glued}$ subunit becomes solubilized, RILP, but not ORP1L, was able to recruit soluble $p150^{Glued}$ to LEs. $p150^{Glued}$ is in fact the most membrane-distal subunit that becomes detached from the Arp1 filament at the base of dynactin after $p50^{dynamitin}$ overexpression (Echeverri et al., 1996; Burkhardt et al., 1997; Ahmad et al., 1998; Eckley et al., 1999). Using $p150^{Glued}$ deletion constructs, we identified the RILP-interacting determinant as the most C-terminal 25-kD part of $p150^{Glued}$. In vitro reconstitution experiments confirmed that RILP, unlike ΔN-RILP or ORP1L, directly interacts with this C-terminal region of $p150^{Glued}$. Thus, the C-terminal half of RILP interacts with GTP–Rab7 and the N-terminal half interacts with the C-terminus of $p150^{Glued}$, and probably with the C-terminus of ORP1L (Fig. 8). The N-terminal half of RILP could not be successfully produced in *E. coli* because of aggregation of the expressed protein and was not recruited to LEs. Thus, a direct interaction of this domain with $p150^{Glued}$ could not be tested. Because both RILP and $p150^{Glued}$ are homodimers, these two proteins may bind as dimer–dimer, but this has not been experimentally verified.

If the Rab7–RILP complex recruits the dynein–dynactin motor complex by directly interacting with $p150^{Glued}$, the function of ORP1L remains elusive. RILP mainly contains coiled-coil

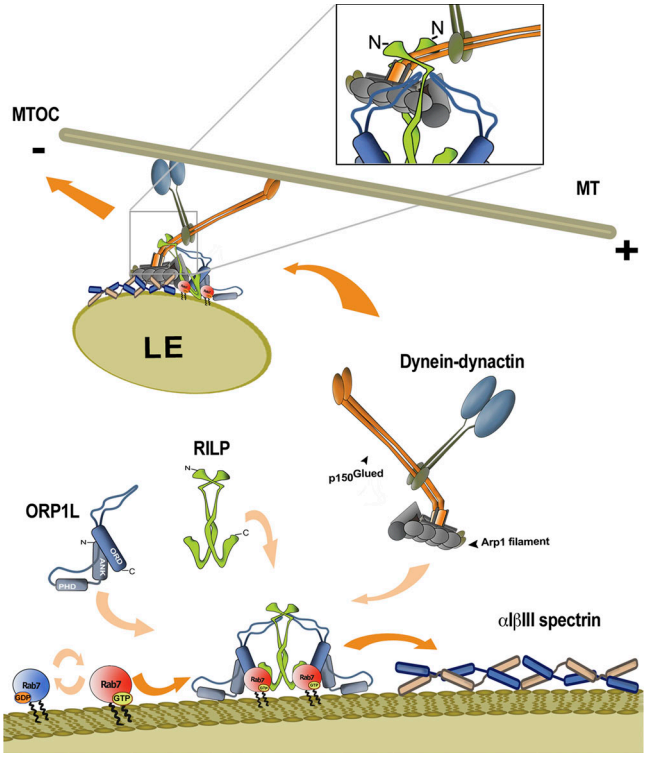

Figure 8. **Model for function of ORP1L in the translocation of the Rab7–RILP–p150^{Glued}–dynein motor complex to βIII spectrin for minus-end transport.** Active GTP-loaded Rab7 localizes to membranes of LEs and recruits the effectors RILP and ORP1L to form a dimer of a heterotrimeric complex. The C-terminal domain of RILP interacts with the switch and interswitch (RabSF1 and RabSF4) regions of Rab7, and the N-terminal half of RILP binds to the C-terminal domain of p150^{Glued} (shown in detail in the box). Subsequently, the 2.4-MD dynein–dynactin motor is recruited by the 0.35-MD ORP1L–Rab7–RILP complex on LEs. ORP1L is required to direct the entire complex to the 0.6-MD αIβIII spectrin. The interaction is mediated by Arp1 binding to βIII spectrin. αIβIII spectrin localizes to several different compartments, but it is not sufficient on its own to recruit dynein motors. Microtubule-based, dynein motor–driven minus-end transport of LEs can only occur after the specific late endocytic dynein receptor Rab7–RILP has interacted with the general dynein membrane receptor βIII spectrin, a process that is facilitated by ORP1L.

regions, whereas ORP1L is composed of multiple defined domains, including three ankyrin repeats, a PH domain, and an oxysterol-binding domain. Both βIII spectrin and ORP1L contain a PH domain with similar specificity (Rameh et al., 1997; Johansson et al., 2005). It is possible that ORP1L is required for Rab7–RILP–dynein motor targeting to specific microdomains on LEs to deliver the dynein motor to its spectrin receptor. This is likely to be the 622-kD αIβIII spectrin heterodimer (Stankewich et al., 1998; De Matteis and Morrow, 2000), which remains bound to late endosomes when RILP is inactivated (Fig. 7 A). The 272-kD βIII spectrin protein contains two Arp1-binding sites (Holleran et al., 2001), repeat regions involved in several protein–protein interactions and a C-terminal PH domain (De Matteis and Morrow, 2000). Via its various molecular interactions, spectrin is strongly associated with multiple membrane compartments, including LEs. Using RNAi, we show that βIII spectrin is critical for minus-end dynein-mediated transport of LEs. Surprisingly, inactivation of ORP1L or βIII spectrin prevented minus-end dynein-mediated transport of LEs, even when Rab7–RILP recruited the p150^{Glued} subunit of dynactin onto the membranes of LEs. The similarity of phenotypes suggests that ORP1L and spectrin are functionally connected. ORP1L could interact directly with αIβIII spectrin, perhaps via its ankyrin repeats. Because the PH domains of ORP1L and βIII spectrin have overlapping specificities (Rameh et al., 1997; Johansson et al., 2005), ORP1L may also transfer the Rab7–RILP–p150^{Glued} complex to the correct microdomains for docking the dynein motor on βIII spectrin. This transfer could be required for dynein motor activation by an unknown mechanism.

In addition, such microdomains may contain a GTPase-activating protein to inactivate GTP–Rab7 and dissociate the RILP–dynein motor complex from LEs. This may be essential because a kinesin and/or dynein motor should be cyclically recruited or activated to drive the bidirectional transport of LEs in a stop-and-go fashion (Wubbolts et al., 1999). How the kinesin motor is recruited and whether this requires dissociation of the Rab7–RILP–dynein motor complex is unclear. Kinesin II can associate with p150^{Glued} (Deacon et al., 2003; Gross, 2003), and the bidirectional movement may be driven by alternating activities of the kinesin and dynein motors on the ORP1L–Rab7–RILP-recruited–p150^{Glued} complex docked on βIII spectrin, which acts as a receptor for both motor activities.

Based on the data presented here, we propose the following model for Rab7-controlled recruitment of the dynein motor complex to its receptor αIβIII spectrin on LEs (Fig. 8). After GTP binding, Rab7 is recruited to late endocytic membranes. Active Rab7 binds two proteins with different functions. The RILP homodimer binds to the switch and interswitch regions of Rab7, arresting Rab7 in the active membrane-bound state (Jordens et al., 2001; Wu et al., 2005; Marsman et al., 2006). ORP1L binding to Rab7 is stabilized by RILP to form a 360-kD complex. Within this complex, the RILP dimer associates with the base of p150^{Glued} to facilitate the recruitment of the dynein–dynactin motor. ORP1L then targets the Rab7–RILP–dynein motor complex to the spectrin receptor on LEs. ORP1L and βIII spectrin are both required for a functional dynein motor, suggesting that RILP-mediated recruitment of the dynein motor to LEs does not suffice for correct docking on the LE–dynein receptor βIII spectrin. The dynein motor is apparently only activated with full cooperation of Rab7, RILP, and ORP1L. The complicated bidirectional motility of LEs is regulated by networks of macromolecular complexes controlled by the small GTPase Rab7.

Materials and methods

cDNA constructs and vectors

ORP1L, RILP, ΔN-RILP, and Rab7 cDNA constructs have been previously described (Fig. 1 A; Jordens et al., 2001; Johansson et al., 2003, 2005; Marsman et al., 2004). The mammalian expression vectors used were pcDNA4HisMax (Invitrogen), pcDNA3.1 (Invitrogen), and pEGFP-C (BD Biosciences). The mRFP–RILP and mRFP–Rab7 fusion constructs were generated by amplification of full-length mRFP by PCR (template plasmid provided by R.Y. Tsien, University of California, San Diego, La Jolla, CA) using forward primer 5′-CCCAGCTAGCACCACCATGGCCTCCTCCGAGGACGTCAT-3′ and reverse primer 5′-GAAGATCTGGCGCCGGTGGAGTG-3′. The mRFP fragment was ligated into the NheI and BglII sites in vector pEGFP-C1, from which the GFP moiety had been removed. The GFP–Arp1 construct was a gift from C. Hoogenraad (Erasmus Medical Centre,

Rotterdam, Netherlands). The C-terminal fragments of $p150^{Glued}$ encoding aa 887–1,278 and 1,049–1,278 were generated by PCR and ligated into the EcoRI and BamHI sites of vector pEGFP-C2 (CLONTECH Laboratories, Inc.). For production of MBP–$p150^{Glued}$ fusion proteins, the same fragments were cloned into the EcoRI and BamHI sites of vector pMAL-c2X (New England Biolabs). A pSUPER vector coexpressing mRFP (Bergink et al., 2006) was used to express short hairpins to down-regulate human βIII spectrin (the sequence targeted by the expressed RNAi is 5′-CGTGGCACGGCTCTGGGAC-3′). siRNA for human RILP was obtained from Dharmacon (ON-TARGETplus SMARTpool for accession no. NP_113618) and cotransfected with a vector expressing GFP–ORP1L (Johansson et al., 2005), using DharmaFECT 1 transfection reagent (Dharmacon). Human ORP1L siRNA oligos with sequence 5′-UrGrCrCrArGUrGrCrCrGrGrAUUrCUrGrATT -3′ were obtained from Proligo and were cotransfected with a vector expressing GFP–RILP (Marsman et al., 2006) using Lipofectamine 2000 (Invitrogen).

For production of hexahistidine (His_6)-tagged proteins, full-length Rab7, or Rab7Q67L, cDNAs were subcloned into the BamHI and XhoI sites of pET-28a (Novagen). A cDNA fragment encoding full-length RILP was subcloned into the NcoI–HindIII sites of vector pETM-11 (a gift from G. Stier, European Molecular Biology Laboratory, Heidelberg, Germany) for production of His_6-tagged RILP. ΔN-RILP was subcloned as a BglII fragment into a BamHI-digested vector pRSET-C (Invitrogen).

Vector pRP265, which is a derivative of pGEX-2T (GE Healthcare) with a modified multiple cloning site, was used to generate GST–Rab7 fusion protein. Full-length ORP1L, ORP1S, and ANK fragment inserts were subcloned into the BamHI site of vector pGEX-1λT (GE Healthcare) for production of GST fusion proteins. Constructs are depicted in Fig. 1 A.

Antibodies

GST–ORP1 and GST–RILP fusion proteins were used for generation of rabbit polyclonal antibodies (Jordens et al., 2001; Johansson et al., 2003, 2005). The other antibodies used were chicken anti-Rab7 (a gift from A. Wandinger-Ness, University of New Mexico, Albuquerque, NM), rabbit anti-Rab7 (Santa Cruz Biotechnology, Inc.), rabbit anti–human αI spectrin and rabbit anti–human βIII spectrin (Santa Cruz Biotechnology, Inc.), mouse anti-Xpress (Invitrogen), mouse anti-myc (Santa Cruz Biotechnology, Inc.), mouse anti-$p150^{Glued}$ (BD Biosciences), HRP-conjugated monoclonal anti-MBP (New England Biolabs), and polyclonal goat anti-GST (GE Healthcare).

Protein purification

His_6-tagged RILP was produced in the *E. coli* strain Rosetta (DE3) pLysS (Novagen) in autoinduction high-density shaking cultures (Studier, 2005) at 24°C for 20 h. Cells were collected and resuspended in buffer A (25 mM Hepes, pH 7.5, 300 mM NaCl, Complete EDTA-free Protease Inhibitor Cocktail [Roche], 1 mM PMSF, 5 mM β-mercaptoethanol, 10 mM imidazole, and 0.05% [vol/vol] Triton X-100), and then lysed by sonication on ice. The cleared lysate was incubated with preequilibrated Talon Co^{2+} resin (CLONTECH Laboratories, Inc.) for 1 h. The resin was packed into a column and washed with buffer A containing 20 mM imidazole, and His_6-RILP was eluted by a step-gradient of imidazole in buffer A. The eluted protein was concentrated in 25 mM Hepes, pH 7.5, 300 mM NaCl, and 10% (vol/vol) glycerol in 10-kD cut-off concentrators (Vivaspin-2; Sartorius).

GST–ORP1L was produced in a similar manner at an induction temperature of 30°C for 18 h. Cells were harvested and lysed in buffer B (25 mM Hepes, pH 8.0, 150 mM NaCl, 1 mM PMSF, Complete Protease Inhibitor Cocktail, 0.1% Triton X-100, and 1 mM DTT). The soluble fraction was combined with glutathione–Sepharose 4B beads (GE Healthcare) and washed extensively with buffer (25 mM Hepes, pH 7.6, and 100 mM NaCl), and the protein was eluted with 15 mM reduced glutathione. The protein was concentrated in 25 mM Hepes, pH 7.6, 150 mM NaCl, 15% (vol/vol) glycerol, and 1 mM DTT.

GST–ANK expression was induced in BL21(DE3) (Stratagene) with 1.0 mM IPTG for 4 h at 37°C. Cells were harvested, resuspended in PBS, and lysed by freeze–thaw cycles followed by sonication. The cleared lysate was incubated with glutathione–Sepharose 4B and washed with PBS, and the protein was eluted with 20 mM reduced glutathione in PBS.

His_6-tagged Rab7 and His_6-tagged Rab7Q67L were expressed in BL21(DE3) (Stratagene) by induction with 0.5 mM IPTG for 5 h at 30°C. After harvesting, the cells were resuspended in 25 mM Hepes, pH 8.0, 300 mM NaCl, 5 mM $MgCl_2$, Complete EDTA-free Protease Inhibitor Cocktail, 1 mM PMSF, 5 mM β-mercaptoethanol, and 10 mM imidazole, and lysed by sonication on ice. The clarified lysates were passed through a HiTrap Chelating HP column (GE Healthcare) charged with Co^{2+} and further purified using a HiTrap SP HP column (GE Healthcare) in 20 mM Mes, pH 6.0, 100 mM NaCl, 5 mM $MgCl_2$, and 5 mM β-mercaptoethanol.

E. coli BL21(DE3) cells harboring the GST–Rab7 construct were induced with 0.5 mM IPTG for 5 h at 30°C. Cells were harvested, resuspended in a buffer containing 50 mM Tris-HCl, pH 7.5, 200 mM NaCl, 1 mM PMSF, Complete EDTA-Free Protease Inhibitor Cocktail, 5 mM $MgCl_2$, and 1 mM DTT, and lysed by sonication on ice. The cleared lysate was loaded on a preequilibrated GSTrap FF column (GE Healthcare) and washed extensively with the same buffer. GST–Rab7 was eluted with 50 mM Tris-HCl, pH 8.0, 100 mM NaCl, 5 mM $MgCl_2$, 1 mM DTT, and 20 mM reduced glutathione.

The MBP–$p150^{Glued}$ fusion proteins were expressed in *E. coli* strain Rosetta (DE3) pLysS (Novagen) and affinity purified using an amylose resin column (New England Biolabs) according to the manufacturer's instructions. All fusion proteins made were analyzed by SDS-PAGE and Coomassie staining; they are depicted in Fig. 1 B.

Immunoprecipitations

Transfected HeLa cells ($\sim 2 \times 10^6$) were washed with ice-cold PBS and scraped into 400 μl of lysis buffer (20 mM Hepes, pH 7.6, 150 mM NaCl, 2 mM $MgCl_2$, 10% glycerol, 0.5% Triton X-100, and 1 mM DTT) with Complete EDTA-free Protease Inhibitor Cocktail. Cells were kept on ice for 15 min and centrifuged for 15 min at 16,000 *g* at 4°C, and the supernatant was preadsorbed at 4°C for 30 min with 30 μl of protein G–Sepharose 4 Fast Flow (GE Healthcare). The recovered supernatant was incubated with Xpress or irrelevant control antibodies at 4°C overnight. The lysate–antibody mixture was incubated at 4°C with protein G–Sepharose for 4 h, followed by washing with lysis buffer. For immunoprecipitation of endogenous ORP1L from HeLa lysates, cells ($\sim 10^7$) were lysed and preadsorbed as described for supernatant. The recovered supernatant was incubated with RILP or irrelevant control antibodies at 4°C for 2 h. The lysate–antibody mixture was incubated at 4°C with protein G–Sepharose for 2 h, followed by washing with lysis buffer. The immunoprecipitates were analyzed by SDS-PAGE and Western blotting.

Pull-down of endogenous RILP

100 μg GST–ORP1L fusion protein and an approximately equimolar amount of 25 μg GST were coupled to 30 μl glutathione–Sepharose 4B beads in coupling buffer (PBS, 2 mM $MgCl_2$, and 1 mM DTT) for 2 h at 4°C. Beads were washed with coupling buffer and equilibrated in lysis buffer (20 mM Hepes, pH 7.6, 150 mM NaCl, 2 mM $MgCl_2$, 10% glycerol, 0.5% Triton X-100, and 1 mM DTT). HeLa cells were lysed as described in the immunoprecipitations section. After centrifugation of the lysates for 15 min at 16,000 *g* at 4°C, the supernatant was added to the beads and incubated for 2 h at 4°C. Beads were washed extensively with lysis buffer, and bound proteins were eluted with 20 mM glutathione. The eluted proteins were analyzed by SDS-PAGE and Western blotting.

Pull-down of in vitro–translated fragments

^{35}S-labeled full-length and truncated proteins were generated by in vitro transcription/translation using the TnT coupled reticulocyte system (Promega) according to the manufacturer's instructions. 50 μg wild-type GST–Rab7 fusion protein was coupled to 20 μl glutathione–Sepharose 4B beads in coupling buffer (PBS, 2 mM $MgCl_2$, and 1 mM DTT) for 2 h at 4°C. Beads were washed with coupling buffer and equilibrated in 20 mM Hepes, pH 7.5, 100 mM KAc, 0.5 mM $MgCl_2$, 1 mM DTT, 2 mM EDTA, and 10 mg/ml albumin. The beads were incubated with 10 μM GTP for 10 min at room temperature, after which $MgCl_2$ was added to a final concentration of 10 mM and the incubation was continued for an additional 30 min. Purified His_6–RILP, His_6–ΔN-RILP, or GST–ORP1L (0 ng, 100 ng, 1 μg, and 5 μg) and in vitro–translated proteins (22 μl) were added to the beads and incubated in a total volume of 0.5 ml for 2 h at 4°C. Beads were washed extensively with wash buffer (20 mM Hepes, pH 7.5, 100 mM KAc, 5 mM $MgCl_2$, and 1 mM DTT), and proteins were eluted with 20 mM glutathione in wash buffer and resolved by SDS-polyacrylamide gels, which were exposed on x-ray film (Kodak) or analyzed by phosphor imaging (FLA-3000; Fujifilm).

Pull-down of purified ORP1L

50 μg His_6–RILP and 50 μg His_6–Rab7Q67L were coupled to 20 μl Talon Co^{2+} resin (CLONTECH Laboratories, Inc.) in coupling buffer (20 mM Hepes, pH 7.5, 150 mM NaCl, 2 mM $MgCl_2$, 10% glycerol, and 5 mM β-mercaptoethanol) for 1 h at 4°C. Beads were washed and equilibrated in coupling buffer with 10 mM imidazole. 2.3 μg purified GST–ORP1L or 5 μg plain GST was added to the beads and incubated for 2 h at 4°C. Beads were

washed extensively with binding buffer (20 mM Hepes, pH 7.5, 150 mM NaCl, 2 mM $MgCl_2$, 10% glycerol, 5 mM β-mercaptoethanol, and 10 mM imidazole) and eluted with 750 mM imidazole in 20 mM Hepes, pH 7.5, 150 mM NaCl, 10% glycerol, and 5 mM β-mercaptoethanol. Samples were analyzed by SDS-PAGE and Western blotting.

Pull-down of purified His_6–RILP

100 μg GST–ANK was coupled to glutathione–Sepharose 4B beads in PBS for 2 h at 4°C, after which the beads were washed and equilibrated in binding buffer (20 mM Hepes, pH 7.5, 150 mM NaCl, 2 mM $MgCl_2$, 10% glycerol, 0.5% Triton X-100, and 1 mM DTT). 10 μg purified His_6–RILP and/or 20 μg His_6–Rab7Q67L were added to the beads and incubated for 4 h at 4°C. Beads were washed with binding buffer and eluted with 20 mM glutathione (30 μl) in binding buffer. Samples were analyzed by SDS-PAGE and Western blotting.

$p150^{Glued}$-binding assay

30 μg GST–Rab7 was coupled to 15 μl glutathione–Sepharose 4B beads and preloaded with GTPγS as described for the pull-down of in vitro–translated fragments. Beads were washed to remove unbound proteins, and recombinant purified His_6–RILP (3 μg), His_6–ΔN-RILP (2 μg), or GST–ORP1L (8 μg) was added to the beads and incubated in a total volume of 0.4 ml for 2 h at 4°C. Beads were washed extensively with detergent/salt buffer (20 mM Hepes, pH 7.5, 300 mM NaCl, 1 mM DTT, 2 mM $MgCl_2$, and 0.1% [vol/vol] Triton X-100), and 4 μg of either MBP–$p150^{Glued}$ (aa 887–1,278) or MBP–$p150^{Glued}$ (aa 1,049–1,278) was added to the beads. Proteins were incubated further in a total volume of 0.4 ml of detergent/salt buffer for 30 min at 22°C. Beads were washed and proteins bound to GTP–Rab7 were eluted by supplementing the 0.4 ml of detergent/salt reaction buffer with EDTA to a final concentration of 20 mM. To precipitate the MBP–$p150^{Glued}$ C25 fusion (aa 1,049–1,278), the elution fractions were combined with 20 μl of amylose resin and incubated for 1 h at 4°C. The resin was washed extensively with detergent/salt buffer before analysis by SDS-PAGE and Western blotting.

Immunofluorescence microscopy

Transfected cells were fixed either with 4% formaldehyde in PBS for 30 min and permeabilized for 5 min with 0.05% Triton X-100 in PBS or with methanol (−20°C) for 5 min. Nonspecific binding of antibodies was blocked by 10% FBS/PBS for 30 min, after which cells were incubated with primary antibody in 5% FBS/PBS for 30 min at 37°C. Bound primary antibodies were visualized with Alexa Fluor secondary antibody conjugates (Invitrogen). Cells were mounted in Mowiol (Calbiochem) containing 50 mg/ml 1,4-diazocyclo-[2,2,2]octane (Sigma-Aldrich) or in Vectashield mounting medium (Vector Laboratories). The specimens were analyzed with confocal laser scanning microscopes (TCS SP1 or TCS SP2) equipped with HCX PL APO and HCX PL APO lbd.bl 40×/NA 1.32 objective lenses (all Leica). The acquisition software used was Leica LCS.

FLIM

FLIM experiments were performed at 37°C in a 5% CO_2 culture hood on an inverted microscope (DM-IRE2; Leica) fitted with a TCS SP2 scanhead and HCX PL APO lbd.bl 40×/NA 1.32 objective lenses and equipped with Lambert Instruments frequency domain lifetime attachment, controlled by EZflim software (Lambert Instruments). Cells were cultured in Delta T dishes (Bioptechs) in CBS medium (140 mM NaCl, 5 mM KCl, 2 mM $MgCl_2$, 1 mM $CaCl_2$, 23 mM $NaHCO_3$, 10 mM [D-]glucose, and 10 mM Hepes, pH 7.3, under 5% CO_2 condition). GFP was excited with ∼4 mW of 488-nm light from a LED modulated at 40 MHz, and emission was collected at 490−550 nm using an intensified charge-coupled device camera (CoolSNAP HQ; Roper Scientific). To calculate the GFP lifetime, the intensities from 40 phase-shifted images (modulation depth ∼70%) were fitted with a sinus function, and lifetimes were derived from the phase shift between excitation and emission. For internal control, cells were cocultured with Mel JuSo cells expressing H2B–GFP only. Lifetimes were referenced to a 1-μM solution of rhodamine-G6 in saline that was set at a 4.11-ns lifetime. The donor FRET efficiency E_D was calculated as $E_D = 1 -$ (measured lifetime/GFP lifetime in control cells) (Zwart et al., 2005).

We are grateful to Seija Puomilahti and Pirjo Ranta for skilled technical assistance. Angela Wandinger-Ness, Roger Y. Tsien, Casper Hoogenraad, and Gunther Stier are acknowledged for providing antibodies and cDNA constructs; Ira Mellman, Marije Marsman, and Peter Peters for support and critical reading of the manuscript; and Kees Jalink for help with FLIM.

Marie Johansson was supported by the Helsinki Graduate School of Biotechnology and Molecular Biology, a European Molecular Biology Organization short-term fellowship, The Finnish Cultural Foundation, and the Alfred Kordelin Foundation. Nuno Rocha was supported by a Portuguese Foundation for Science and Technology FCT/ FSE PhD scholarship within the Third Framework Program and a grant from the Dutch Cancer Society KWF. This study was further supported by the Academy of Finland (grants 206298 and 113010), the Sigrid Juselius Foundation, and the Finnish Foundation for Cardiovascular Research (to V.M. Olkkonen).

Submitted: 15 June 2006
Accepted: 9 January 2007

References

Ahmad, F.J., C.J. Echeverri, R.B. Vallee, and P.W. Baas. 1998. Cytoplasmic dynein and dynactin are required for the transport of microtubules into the axon. *J. Cell Biol.* 140:391–401.

Bastiaens, P.I., and A. Squire. 1999. Fluorescence lifetime imaging microscopy: spatial resolution of biochemical processes in the cell. *Trends Cell Biol.* 9:48–52.

Berger, B., D.B. Wilson, E. Wolf, T. Tonchev, M. Milla, and P.S. Kim. 1995. Predicting coiled coils by use of pairwise residue correlations. *Proc. Natl. Acad. Sci. USA*. 92:8259–8263.

Bergink, S., F.A. Salomons, D. Hoogstraten, T.A. Groothuis, H. de Waard, J. Wu, L. Yuan, E. Citterio, A.B. Houtsmuller, J. Neefjes, et al. 2006. DNA damage triggers nucleotide excision repair-dependent monoubiquitylation of histone H2A. *Genes Dev.* 20:1343–1352.

Burkhardt, J.K., C.J. Echeverri, T. Nilsson, and R.B. Vallee. 1997. Overexpression of the dynamitin (p50) subunit of the dynactin complex disrupts dynein-dependent maintenance of membrane organelle distribution. *J. Cell Biol.* 139:469–484.

Cantalupo, G., P. Alifano, V. Roberti, C.B. Bruni, and C. Bucci. 2001. Rab-interacting lysosomal protein (RILP): the Rab7 effector required for transport to lysosomes. *EMBO J.* 20:683–693.

Colucci, A.M., M.C. Campana, M. Bellopede, and C. Bucci. 2005. The Rab-interacting lysosomal protein, a Rab7 and Rab34 effector, is capable of self-interaction. *Biochem. Biophys. Res. Commun.* 334:128–133.

Culver-Hanlon, T.L., S.A. Lex, A.D. Stephens, N.J. Quintyne, and S.J. King. 2006. A microtubule-binding domain in dynactin increases dynein processivity by skating along microtubules. *Nat. Cell Biol.* 8:264–270.

Deacon, S.W., A.S. Serpinskaya, P.S. Vaughan, M. Lopez Fanarraga, I. Vernos, K.T. Vaughan, and V.I. Gelfand. 2003. Dynactin is required for bidirectional organelle transport. *J. Cell Biol.* 160:297–301.

De Matteis, M.A., and J.S. Morrow. 2000. Spectrin tethers and mesh in the biosynthetic pathway. *J. Cell Sci.* 113:2331–2343.

Echeverri, C.J., B.M. Paschal, K.T. Vaughan, and R.B. Vallee. 1996. Molecular characterization of the 50-kD subunit of dynactin reveals function for the complex in chromosome alignment and spindle organization during mitosis. *J. Cell Biol.* 132:617–633.

Eckley, D.M., S.R. Gill, K.A. Melkonian, J.B. Bingham, H.V. Goodson, J.E. Heuser, and T.A. Schroer. 1999. Analysis of dynactin subcomplexes reveals a novel actin-related protein associated with the Arp1 minifilament pointed end. *J. Cell Biol.* 147:307–320.

Förster, T. 1948. Zwischenmolekulare energiewandering und fluoreszenz. *Annalen Physik*. 6:55–75.

Gross, S.P. 2003. Dynactin: coordinating motors with opposite inclinations. *Curr. Biol.* 13:R320–R322.

Harrison, R.E., J.H. Brumell, A. Khandani, C. Bucci, C.C. Scott, X. Jiang, B.B. Finlay, and S. Grinstein. 2004. *Salmonella* impairs RILP recruitment to Rab7 during maturation of invasion vacuoles. *Mol. Biol. Cell*. 15:3146–3154.

Hirokawa, N. 1998. Kinesin and dynein superfamily proteins and the mechanism of organelle transport. *Science*. 279:519–526.

Holleran, E.A., L.A. Ligon, M. Tokito, M.C. Stankewich, J.S. Morrow, and E.L. Holzbaur. 2001. beta III spectrin binds to the Arp1 subunit of dynactin. *J. Biol. Chem.* 276:36598–36605.

Hoogenraad, C.C., A. Akhmanova, S.A. Howell, B.R. Dortland, C.I. De Zeeuw, R. Willemsen, P. Visser, F. Grosveld, and N. Galjart. 2001. Mammalian Golgi-associated Bicaudal-D2 functions in the dynein-dynactin pathway by interacting with these complexes. *EMBO J.* 20:4041–4054.

Hoogenraad, C.C., P. Wulf, N. Schiefermeier, T. Stepanova, N. Galjart, J.V. Small, F. Grosveld, C.I. de Zeeuw, and A. Akhmanova. 2003. Bicaudal D induces selective dynein-mediated microtubule minus end-directed transport. *EMBO J.* 22:6004–6015.

Johansson, M., V. Bocher, M. Lehto, G. Chinetti, E. Kuismanen, C. Ehnholm, B. Staels, and V.M. Olkkonen. 2003. The two variants of oxysterol binding protein-related protein-1 display different tissue expression patterns, have different intracellular localization, and are functionally distinct. *Mol. Biol. Cell*. 14:903–915.

Johansson, M., M. Lehto, K. Tanhuanpaa, T.L. Cover, and V.M. Olkkonen. 2005. The oxysterol-binding protein homologue ORP1L interacts with Rab7 and alters functional properties of late endocytic compartments. *Mol. Biol. Cell*. 16:5480–5492.

Jordens, I., M. Fernandez-Borja, M. Marsman, S. Dusseljee, L. Janssen, J. Calafat, H. Janssen, R. Wubbolts, and J. Neefjes. 2001. The Rab7 effector protein RILP controls lysosomal transport by inducing the recruitment of dynein-dynactin motors. *Curr. Biol.* 11:1680–1685.

Jordens, I., M. Marsman, C. Kuijl, and J. Neefjes. 2005. Rab proteins, connecting transport and vesicle fusion. *Traffic*. 6:1070–1077.

Jordens, I., W. Westbroek, M. Marsman, N. Rocha, M. Mommaas, M. Huizing, J. Lambert, J. Naeyaert, and J. Neefjes. 2006. Rab7 and Rab27a control two motor protein activities involved in melanosomal transport. *Pigment Cell Res.* 19:412–423.

Karki, S., and E.L. Holzbaur. 1999. Cytoplasmic dynein and dynactin in cell division and intracellular transport. *Curr. Opin. Cell Biol.* 11:45–53.

King, S.J., and T.A. Schroer. 2000. Dynactin increases the processivity of the cytoplasmic dynein motor. *Nat. Cell Biol.* 2:20–24.

Kumar, S., Y. Zhou, and M. Plamann. 2001. Dynactin-membrane interaction is regulated by the C-terminal domains of p150(Glued). *EMBO Rep.* 2:939–944.

Lehto, M., and V.M. Olkkonen. 2003. The OSBP-related proteins: a novel protein family involved in vesicle transport, cellular lipid metabolism, and cell signalling. *Biochim. Biophys. Acta*. 1631:1–11.

Lupas, A., M. Van Dyke, and J. Stock. 1991. Predicting coiled coils from protein sequences. *Science*. 252:1162–1164.

Marsman, M., I. Jordens, C. Kuijl, L. Janssen, and J. Neefjes. 2004. Dynein-mediated vesicle transport controls intracellular *Salmonella* replication. *Mol. Biol. Cell*. 15:2954–2964.

Marsman, M., I. Jordens, N. Rocha, C. Kuijl, L. Janssen, and J. Neefjes. 2006. A splice variant of RILP induces lysosomal clustering independent of dynein recruitment. *Biochem. Biophys. Res. Commun.* 344:747–756.

Matanis, T., A. Akhmanova, P. Wulf, E. Del Nery, T. Weide, T. Stepanova, N. Galjart, F. Grosveld, B. Goud, C.I. De Zeeuw, et al. 2002. Bicaudal-D regulates COPI-independent Golgi-ER transport by recruiting the dynein-dynactin motor complex. *Nat. Cell Biol.* 4:986–992.

Mizuno, K., A. Kitamura, and T. Sasaki. 2003. Rabring7, a novel Rab7 target protein with a RING finger motif. *Mol. Biol. Cell*. 14:3741–3752.

Muresan, V., M.C. Stankewich, W. Steffen, J.S. Morrow, E.L. Holzbaur, and B.J. Schnapp. 2001. Dynactin-dependent, dynein-driven vesicle transport in the absence of membrane proteins: a role for spectrin and acidic phospholipids. *Mol. Cell*. 7:173–183.

Navarro, C., H. Puthalakath, J.M. Adams, A. Strasser, and R. Lehmann. 2004. Egalitarian binds dynein light chain to establish oocyte polarity and maintain oocyte fate. *Nat. Cell Biol.* 6:427–435.

Rameh, L.E., A. Arvidsson, K.L. Carraway III, A.D. Couvillon, G. Rathbun, A. Crompton, B. VanRenterghem, M.P. Czech, K.S. Ravichandran, S.J. Burakoff, et al. 1997. A comparative analysis of the phosphoinositide binding specificity of pleckstrin homology domains. *J. Biol. Chem.* 272:22059–22066.

Schroer, T.A. 2004. Dynactin. *Annu. Rev. Cell Dev. Biol.* 20:759–779.

Schroer, T.A., E.R. Steuer, and M.P. Sheetz. 1989. Cytoplasmic dynein is a minus end-directed motor for membranous organelles. *Cell*. 56:937–946.

Short, B., C. Preisinger, J. Schaletzky, R. Kopajtich, and F.A. Barr. 2002. The Rab6 GTPase regulates recruitment of the dynactin complex to Golgi membranes. *Curr. Biol.* 12:1792–1795.

Stankewich, M.C., W.T. Tse, L.L. Peters, Y. Ch'ng, K.M. John, P.R. Stabach, P. Devarajan, J.S. Morrow, and S.E. Lux. 1998. A widely expressed betaIII spectrin associated with Golgi and cytoplasmic vesicles. *Proc. Natl. Acad. Sci. USA*. 95:14158–14163.

Stinchcombe, J.C., E. Majorovits, G. Bossi, S. Fuller, and G.M. Griffiths. 2006. Centrosome polarization delivers secretory granules to the immunological synapse. *Nature*. 443:462–465.

Studier, F.W. 2005. Protein production by auto-induction in high density shaking cultures. *Protein Expr. Purif.* 41:207–234.

Vale, R.D. 2003. The molecular motor toolbox for intracellular transport. *Cell*. 112:467–480.

Wallrabe, H., and A. Periasamy. 2005. Imaging protein molecules using FRET and FLIM microscopy. *Curr. Opin. Biotechnol.* 16:19–27.

Waterman-Storer, C.M., S. Karki, and E.L. Holzbaur. 1995. The p150Glued component of the dynactin complex binds to both microtubules and the actin-related protein centractin (Arp-1). *Proc. Natl. Acad. Sci. USA*. 92:1634–1638.

Wu, M., T. Wang, E. Loh, W. Hong, and H. Song. 2005. Structural basis for recruitment of RILP by small GTPase Rab7. *EMBO J.* 24:1491–1501.

Wubbolts, R., M. Fernandez-Borja, I. Jordens, E. Reits, S. Dusseljee, C. Echeverri, R.B. Vallee, and J. Neefjes. 1999. Opposing motor activities of dynein and kinesin determine retention and transport of MHC class II-containing compartments. *J. Cell Sci.* 112:785–795.

Zwart, W., A. Griekspoor, C. Kuijl, M. Marsman, J. van Rheenen, H. Janssen, J. Calafat, M. van Ham, L. Janssen, M. van Lith, et al. 2005. Spatial separation of HLA-DM/HLA-DR interactions within MIIC and phagosome-induced immune escape. *Immunity*. 22:221–233.